International Journal of Thermal Sciences 179 (2022) 107639

Contents lists available at ScienceDirect

International Journal of Thermal Sciences

journal homepage: www.elsevier.com/locate/ijts

Convection in a differentially heated cubic cavity rolling about horizontal axis

Stepan A. Mikhailenko, Mikhail A. Sheremet *

Laboratory on Convective Heat and Mass Transfer, Tomsk State University, 634050, Tomsk, Russia

ARTICLE INFO

Keywords:
Natural convection
Rotation
Three-dimensional modeling
Centrifugal force

ABSTRACT

Many different engineering systems in electronics, power engineering and medicine are under the rotation influence. Therefore, it is very useful to describe from physical point of view the heat transport features in rotating elements. The present research deals with computational investigation of convective energy transport in a differentially heated rotating cubic chamber. The cavity has a left vertical heated wall and the opposite cold border, while the rest borders are thermally insulated. The basic equations have been formulated using the vector potential functions and vorticity vector. The set of control equations has been worked out by using the finite difference procedures. Temperature and velocity fields for different rotation angles have been shown and described in detail. The influence of the cavity rotation rate and the temperature gradient between the walls has been illustrated using the average Nusselt number. The performed analysis has shown that the centrifugal force influence on heat transfer can be neglected for the considered flow modes using the Boussinesq approximation. A growth of the Taylor number results in a suppression of convective heat transfer in the case of low and moderate values of the Rayleigh number, while for high Rayleigh numbers the rotation has an opposite influence on heat transfer with heat transfer enhancement. Comparison between 2D and 3D outcomes illustrates a presence of some differences between these models due to the restrictive effect of cubical surfaces.

1. Introduction

The task on convective heat and mass transport is very important nowadays and such a phenomenon can be found in various engineering systems. Useful area of research is an energy transport under rotation influence. Rotating units can be discovered in solving many engineering problems, including modeling of the rotary thermal systems [1], growing crystals [2], modeling of the solar concentrators [3], in metallurgy [4], modeling of the cooling complex for electronics [5,6]. For example, alternate rotation of a container with a crystal around a vertical axis contributes to homogeneous melt mixing and improvement hydrodynamic process conditions for crystal growing. Such conditions favorably affect the productivity of the growth process and the perfection of the resulting crystals [2]. Rotating electronic equipment can be found in radar systems, in the space industry and various technically complex devices. Electric motors are also very common today, in which overheating and loss of engine performance due to currents can occur. Therefore, the study of heat transfer under rotation conditions is a useful problem.

So, the energy transport in a finned rotating channel has been investigated experimentally by Huang et al. [1]. Two models of channels with staggered and inline fins position have been considered. It has been revealed that energy transfer in stationary channel is higher by 25–30% for staggered pin-fin arrays in comparison with inline ones. At the same time, rotation has caused the heat transfer enhancement of 93% in the inline case, while for the staggered case one can find only 22%. The influence of rotation on the double-diffusive convection in a silicon liquid bridge has been studied by Le et al. [2]. It has been shown that rotation can augment azimuthal uniformity and decrease the concentration changes. Wu et al. [3] have analyzed natural convection in a rolling chamber for solar concentration systems. The authors have showed that convective losses for solar applications can be reduced by 10% using rotation. Convective energy transport in a differentially warmed rotating cubical chamber saturated with medium of $Pr = 0.0321$ has been performed by Chokri and Brahim [4]. The results have shown that Coriolis forces appear to play a prevailing role in suppressing thermal buoyancy, and increasing of Taylor number can reduce maximum of heat transfer rate. Jin et al. [5] have examined rotating

* Corresponding author.
E-mail address: michael-sher@yandex.ru (M.A. Sheremet).

https://doi.org/10.1016/j.ijthermalsci.2022.107639
Received 11 January 2022; Received in revised form 8 April 2022; Accepted 13 April 2022
Available online 23 April 2022

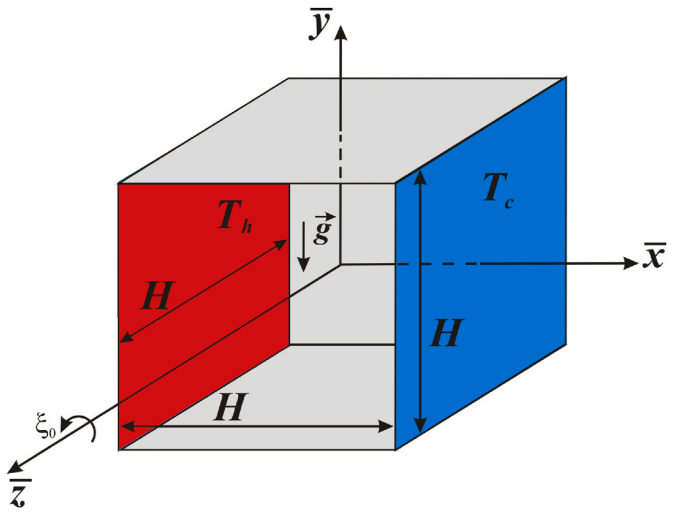

Fig. 1. Problem sketch.

Table 1
Average Nusselt number values with different times.

τ	Results for uniform mesh 120 × 120 × 120	Results for uniform mesh 60 × 60 × 60	Data from Ref. [29] for uniform mesh 40 × 40 × 40	Data from Ref. [29] for uniform mesh 30 × 30 × 30
0.05	4.622	4.747	4.727	4.773
0.10	4.048	4.135	4.152	4.182
0.15	3.89	3.976	3.987	4.020
0.20	3.846	3.935	3.939	3.971
Steady state	3.833	3.921	3.926	3.956

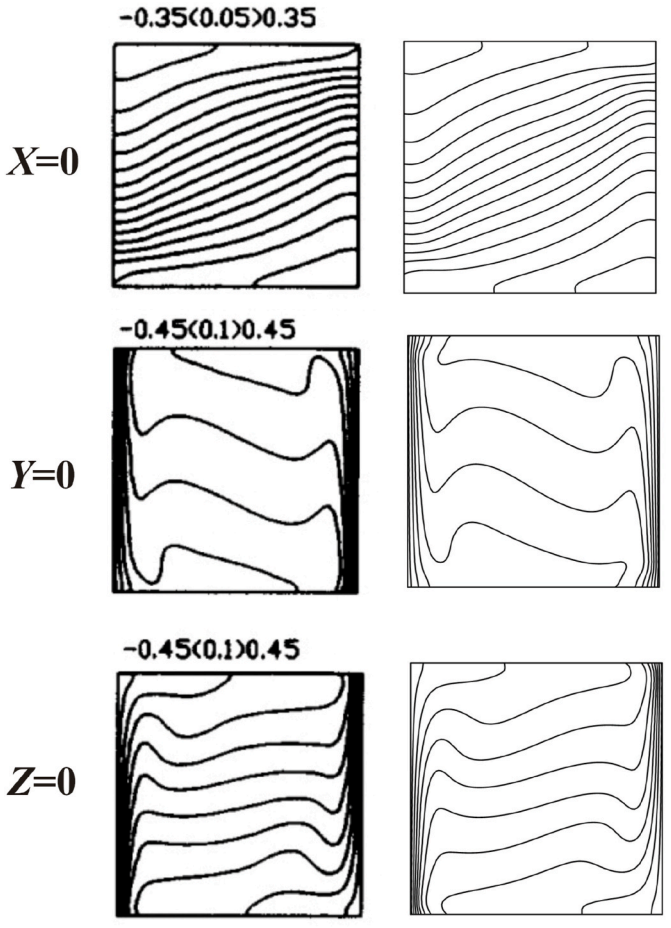

Fig. 2. The comparison of isotherms at different cross-sections for $Ra = 10^6$, $Ta = 10^6$, $Ra_\xi = 10^2$: first column – data from Ref. [29], the second column – obtained results.

heat transfer in a chamber with local energy sources experimentally and numerically. The authors have developed an experimental stand and a numerical simulation program to study the rotating electronics cooling. The authors have noted the periodic phenomena of heat transfer. The influence of centrifugal and Coriolis forces on convective energy transport in two-dimensional differentially heated cavity has been investigated by Tso et al. [6]. The authors have shown that the impact of the Coriolis force is negligible, at the same time sufficient, while the effect of centrifugal force on energy transference is small. Investigation of natural convection in a rolling chamber with heaters has been performed by Jin et al. [7]. Three possible modes of heat transfer have been established including uni-rolling periodic oscillation, multi-rolling periodic oscillation and chaotic oscillation. Al-Zurf et al. [8] have investigated the influence of wavy surfaces on the turbulent forced convection under rotational conditions. The authors considered symmetric and asymmetric sinusoidal wave channels. The RANS method has been used in turbulent flow simulation. Calculations have been carried out for rotating speeds between 0 and 1000 rpm. It has been found that rotation has a strong effect on the flow structure and energy transport parameters. The Coriolis force enhances the energy transference at the bottom wall as the rotation speed increases. Tao et al. [9] have conduced experiments for analysis of rotation influence in a channel with lateral fluid extraction on flow and heat transfer parameters. Experiments have shown that rotation decreases the mean Nusselt number. Natural convection in a rolling porous medium has been investigated by Vanishree and Siddheshwar [10]. A linear stability analysis has been performed by solving the Rayleigh–Bénard equations system with the non-Boussinesq impact of variable viscosity. The influence of the anisotropy parameters on the onset of convective transport with rotation is similar to the case without one. The convection in a long rolling porous box has been investigated by Vadasz [11]. Two types of boundary conditions have been considered including perfectly conducting horizontal walls and adiabatic bottom wall. The fluid motion has been driven by internal heating generation due to perpendicular temperature gradients to the centrifugal body force. The impact of the Coriolis force on the onset of convection in rolling porous media has been investigated by Govender Vadasz [12]. Studies by Yadav [13–15] have been devoted to the convection behavior in rotating porous regions. The author has shown that rotation suspends the appearance of convection, and the start of this phenomenon has been noted with exceeding of the rotation parameter threshold value. Hussain et al. [16] have presented a study on three-dimensional MHD rotational convection of nanofluids across a radiative stretching surface. Tiwari and Das nanofluid model with effective parameters have been used for governing equations formulation. A computational investigation of convective energy and mass transport in a rotating channel has been carried out by Sohankar et al. [17]. The authors considered various boundary thermal conditions including constant temperature and constant thermal flux at the border. Interestingly, in the presence of rotation, the case of constant temperature reflects the Nusselt number higher than for the constant thermal flux, while for the case of motionless channel the behavior is opposite. Shekhar et al. [18] have scrutinized numerically an influence of cross-diffusion on convective energy transport in a rotating sparsely packed porous zone. It has been revealed that the Solutal Rayleigh and Taylor numbers stabilize the considered convective system. Alshomrani et al. [19,20] have studied the convective heat transfer in an inclined cubic box with solid heater and discrete cooling. Various positions of the heat source and cooling zones have been considered at different

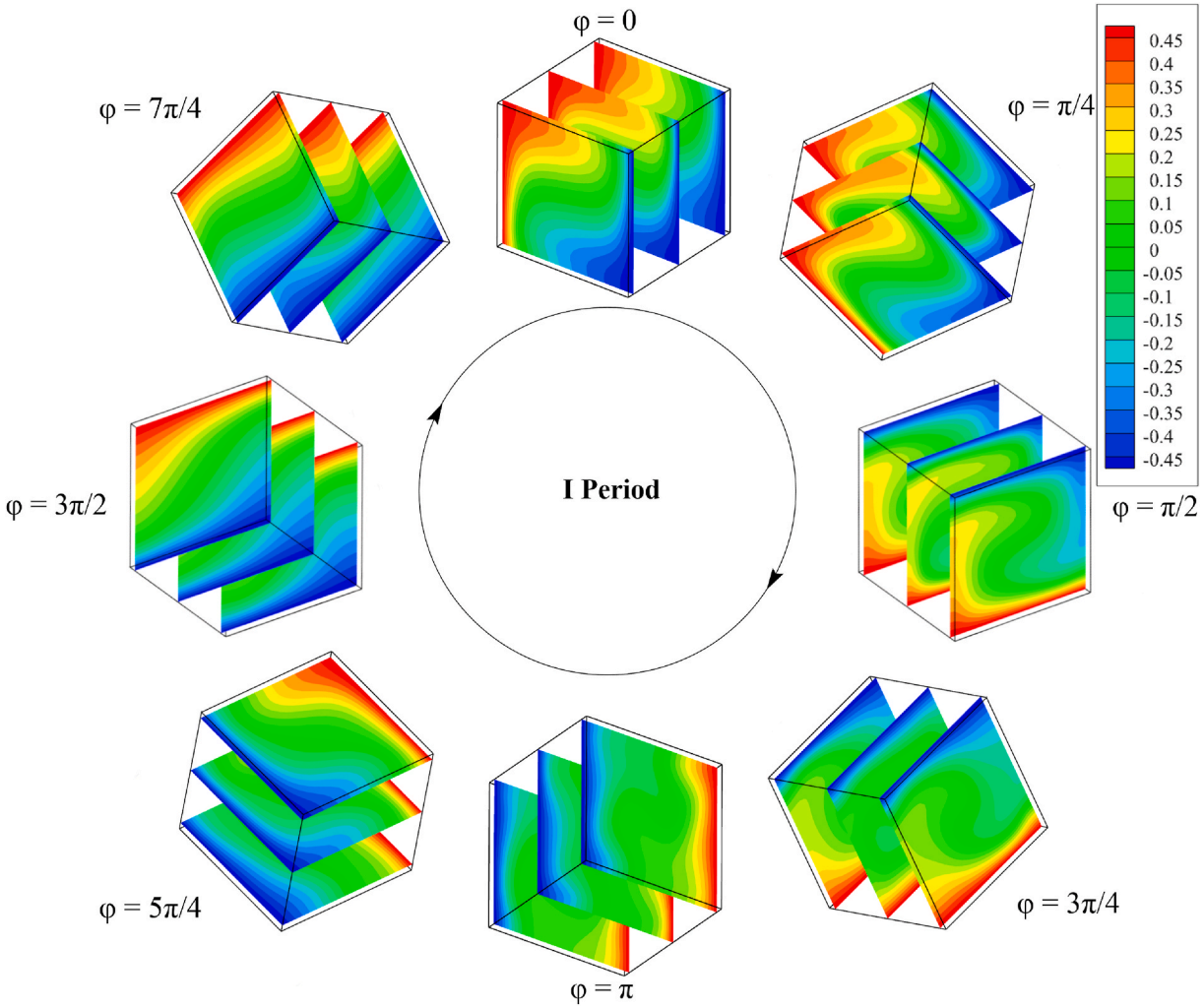

Fig. 3. Temperature fields for cross-sections along z-coordinate at $Ra = 10^5$, $Ta = 10^4$, $Ra_\xi = 1.8{\cdot}10^2$ and different angles of the cavity rotation.

inclination angles of the cubic cavity. It has been shown that the inclination of the cavity and heater/cooler positions strongly influence the flow and heat transfer inside the enclosure.

Heat transfer can be enhanced by using rotating elements within the regions. Such nature has been shown by Kolsi et al. [21], Shirani and Toghraie [22] for rotating cylinders inside partially or completely porous channels. Yang et al. [23] have studied convective heat transfer in rotating metal foam of high porosity. It has been found that rotation has a positive influence on the coefficient of interstitial heat transfer. Ker and Lin [24] have carried out a computational and experimental research of air flow in a cubic rolling chamber. Also, interesting experimental results on the considered topic can be found in [25–28].

This brief review shows the importance of convective energy and mass transference in three-dimensional regions. This problem becomes more topical including the rotation effect, but there are few works devoted to this topic. Therefore, the study of the influence of rotation on thermal convection in a closed cubic cavity with differential heating is carried out in this work and the obtained results have theoretical and practical significance. It should be noted that these outcomes can be used for control of heat removal from the heated units within the rotating systems in electronics and heat exchangers.

2. Basic equations

Convective energy transport is studied in a differentially heated rolling cubical cavity of size H, showed in Fig. 1. The chamber rotates with a fixed angular rate ξ_0 in counterclockwise direction relative to the $\overline{z}$-axis. The vertical boundary ($\overline{x} = -H/2$) is warmed by the temperature T_h, while the right one ($\overline{x} = H/2$) is cooled by the temperature T_c. Other borders of the chamber are thermally insulated. The medium filling the cavity is a Newtonian incompressible liquid of $Pr = 0.7$ satisfying the Boussinesq approximation. All physical parameters of the fluid are independent of temperature. The flow regime is laminar.

Partial differential equations describing the transport phenomena in a rotating cubical cavity have the form of Oberbeck-Boussinesq equations with rotation influence:

$$\frac{\partial \overline{u}}{\partial \overline{x}} + \frac{\partial \overline{v}}{\partial \overline{y}} + \frac{\partial \overline{w}}{\partial \overline{z}} = 0 \tag{1}$$

$$\rho\left(\frac{\partial \overline{u}}{\partial t} + \overline{u}\frac{\partial \overline{u}}{\partial \overline{x}} + \overline{v}\frac{\partial \overline{u}}{\partial \overline{y}} + \overline{w}\frac{\partial \overline{u}}{\partial \overline{z}}\right) = -\frac{\partial p}{\partial \overline{x}} + \mu\left(\frac{\partial^2 \overline{u}}{\partial \overline{x}^2} + \frac{\partial^2 \overline{u}}{\partial \overline{y}^2} + \frac{\partial^2 \overline{u}}{\partial \overline{z}^2}\right) + \\ +\rho\beta(T - T_c)g\sin(\xi_0 t) - \rho\beta(T - T_c)\xi_0^2\overline{x} + 2\rho\overline{v}\xi_0 \tag{2}$$

$$\rho\left(\frac{\partial \overline{v}}{\partial t} + \overline{u}\frac{\partial \overline{v}}{\partial \overline{x}} + \overline{v}\frac{\partial \overline{v}}{\partial \overline{y}} + \overline{w}\frac{\partial \overline{v}}{\partial \overline{z}}\right) = -\frac{\partial p}{\partial \overline{y}} + \mu\left(\frac{\partial^2 \overline{v}}{\partial \overline{x}^2} + \frac{\partial^2 \overline{v}}{\partial \overline{y}^2} + \frac{\partial^2 \overline{v}}{\partial \overline{z}^2}\right) + \\ +\rho\beta(T - T_c)g\cos(\xi_0 t) - \rho\beta(T - T_c)\xi_0^2\overline{y} - 2\rho\overline{u}\xi_0 \tag{3}$$

$$\rho\left(\frac{\partial \overline{w}}{\partial t} + \overline{u}\frac{\partial \overline{w}}{\partial \overline{x}} + \overline{v}\frac{\partial \overline{w}}{\partial \overline{y}} + \overline{w}\frac{\partial \overline{w}}{\partial \overline{z}}\right) = -\frac{\partial p}{\partial \overline{z}} + \mu\left(\frac{\partial^2 \overline{w}}{\partial \overline{x}^2} + \frac{\partial^2 \overline{w}}{\partial \overline{y}^2} + \frac{\partial^2 \overline{w}}{\partial \overline{z}^2}\right) \tag{4}$$

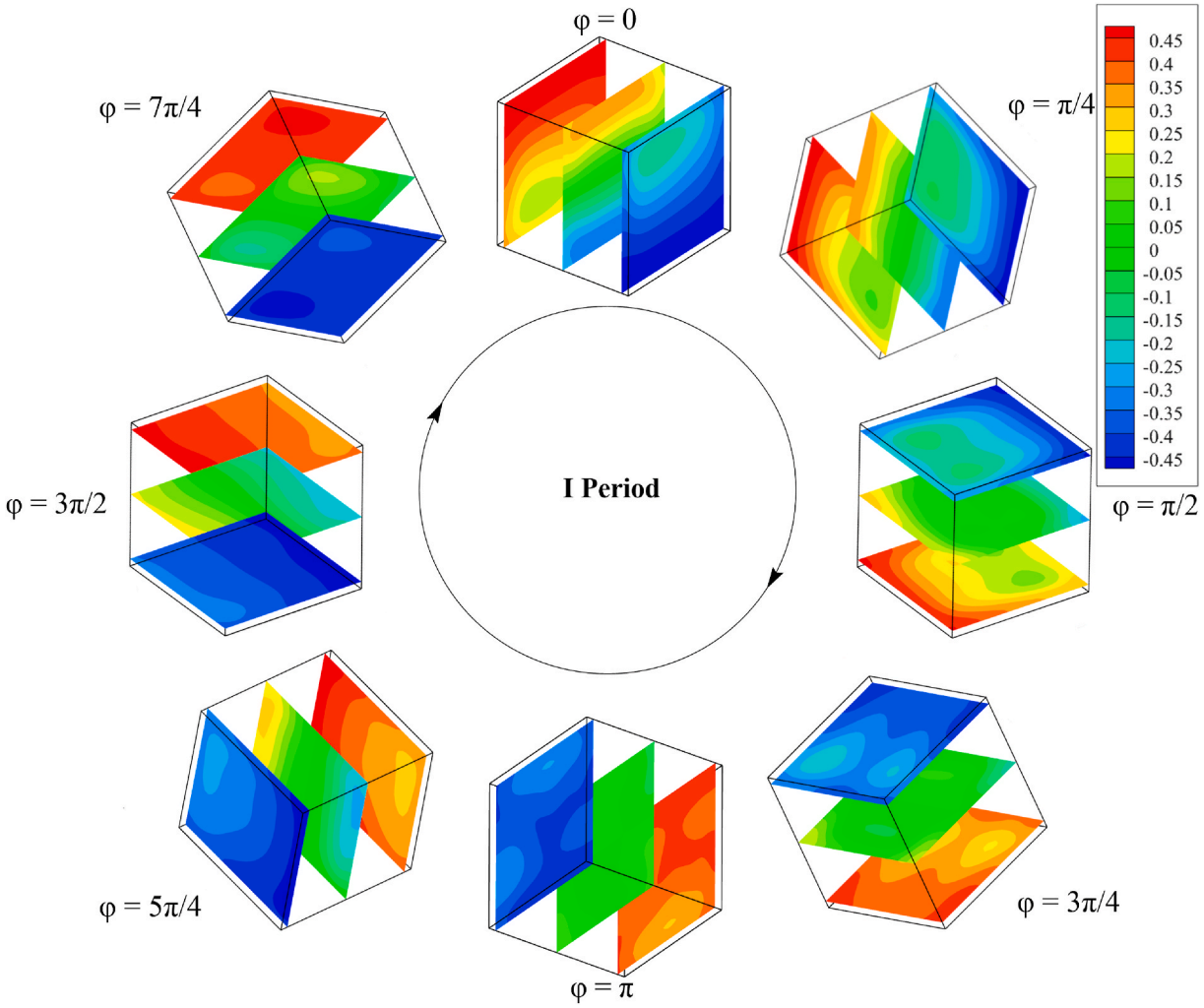

Fig. 4. Temperature fields for cross-sections along x-coordinate at $Ra = 10^5$, $Ta = 10^4$, $Ra_\xi = 1.8{\cdot}10^2$ and different angles of the cavity rotation.

$$\frac{\partial T}{\partial t}+\overline{u}\frac{\partial T}{\partial \overline{x}}+\overline{v}\frac{\partial T}{\partial \overline{y}}+\overline{w}\frac{\partial T}{\partial \overline{z}}=\frac{k_f}{(\rho c)_f}\left(\frac{\partial^2 T}{\partial \overline{x}^2}+\frac{\partial^2 T}{\partial \overline{y}^2}+\frac{\partial^2 T}{\partial \overline{z}^2}\right) \tag{5}$$

It should be noted that these equations (1)–(5) have been obtained in the case of relative motion when the coordinate system $O\overline{x}\overline{y}\overline{z}$ is related with the rotating cavity. As a result the motion equations (2) and (3) include the rotational buoyancy or centrifugal force (the fourth term on the right of equation) and Coriolis force (the last term on the right of equation).

The additional restrictions are.

- $\overline{u}=\overline{v}=\overline{w}=0$, $T=T_h$ at the heated surface $\overline{x}=-H/2$;
- $\overline{u}=\overline{v}=\overline{w}=0$, $T=T_c$ at the cooled surface $\overline{x}=H/2$;
- $\overline{u}=\overline{v}=\overline{w}=0$, $\frac{\partial T}{\partial \overline{y}}=0$ at the adiabatic surfaces $\overline{y}=\pm H/2$;
- $\overline{u}=\overline{v}=\overline{w}=0$, $\frac{\partial T}{\partial \overline{z}}=0$ at the adiabatic surfaces $\overline{z}=\pm H/2$.

Introducing vector potential functions $\left(\overline{u}=\frac{\partial \overline{\psi}_z}{\partial \overline{y}}-\frac{\partial \overline{\psi}_y}{\partial \overline{z}},\ \overline{v}=\frac{\partial \overline{\psi}_x}{\partial \overline{z}}-\frac{\partial \overline{\psi}_z}{\partial \overline{x}},\ \overline{w}=\frac{\partial \overline{\psi}_y}{\partial \overline{x}}-\frac{\partial \overline{\psi}_x}{\partial \overline{y}}\right)$, vorticity vector $\left(\overline{\omega}_x=\frac{\partial \overline{w}}{\partial \overline{y}}-\frac{\partial \overline{v}}{\partial \overline{z}},\ \overline{\omega}_y=\frac{\partial \overline{u}}{\partial \overline{z}}-\frac{\partial \overline{w}}{\partial \overline{x}},\ \overline{\omega}_z=\frac{\partial \overline{v}}{\partial \overline{x}}-\frac{\partial \overline{u}}{\partial \overline{y}}\right)$ and non-dimensional variables $x=\overline{x}/H$, $y=\overline{y}/H$, $\tau=\xi_0 t$, $u=\overline{u}/(\xi_0 H)$, $v=\overline{v}/(\xi_0 H)$, $\psi=\overline{\psi}/(\xi_0 H^2)$, $\theta=(T-T_c)/\Delta T$ the resulting set of the control equations is

$$\nabla^2\psi_x=-\omega_x,\ \nabla^2\psi_y=-\omega_y,\ \nabla^2\psi_z=-\omega_z \tag{6}$$

$$\frac{\partial \omega_x}{\partial \tau}+u\frac{\partial \omega_x}{\partial x}+v\frac{\partial \omega_x}{\partial y}+w\frac{\partial \omega_x}{\partial z}-\omega_x\frac{\partial u}{\partial x}-\omega_y\frac{\partial u}{\partial y}-\omega_z\frac{\partial u}{\partial z}= =\frac{1}{\sqrt{Ta}}\left(\frac{\partial^2 \omega_x}{\partial x^2}+\frac{\partial^2 \omega_x}{\partial y^2}+\frac{\partial^2 \omega_x}{\partial z^2}\right)-\frac{Ra}{Pr{\cdot}Ta}\frac{\partial \theta}{\partial z}\cos(\tau)+\frac{Ra_\xi}{Pr{\cdot}Ta}y\frac{\partial \theta}{\partial z}+2\frac{\partial u}{\partial z} \tag{7}$$

$$\frac{\partial \omega_y}{\partial \tau}+u\frac{\partial \omega_y}{\partial x}+v\frac{\partial \omega_y}{\partial y}+w\frac{\partial \omega_y}{\partial z}-\omega_x\frac{\partial v}{\partial x}-\omega_y\frac{\partial v}{\partial y}-\omega_z\frac{\partial v}{\partial z}= =\frac{1}{\sqrt{Ta}}\left(\frac{\partial^2 \omega_y}{\partial x^2}+\frac{\partial^2 \omega_y}{\partial y^2}+\frac{\partial^2 \omega_y}{\partial z^2}\right)+\frac{Ra}{Pr{\cdot}Ta}\frac{\partial \theta}{\partial z}\sin(\tau)-\frac{Ra_\xi}{Pr{\cdot}Ta}x\frac{\partial \theta}{\partial z}+2\frac{\partial v}{\partial z} \tag{8}$$

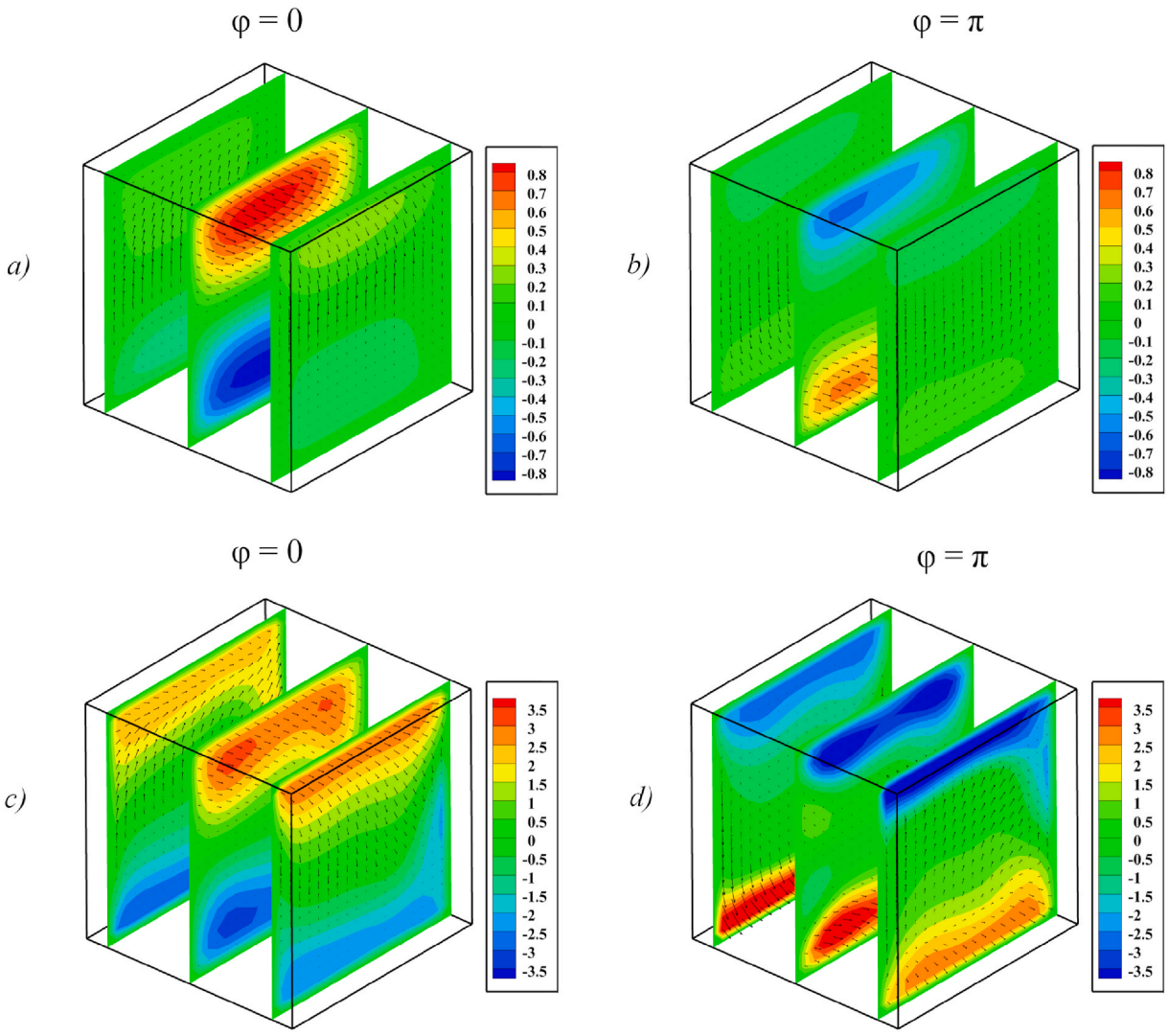

Fig. 5. Vertical velocity patterns for cross-sections along x-coordinate at $Ta = 10^3$ and different Ra and φ: *a)* $Ra = 10^4$ and $\varphi = 0$, *b)* $Ra = 10^4$ and $\varphi = \pi$, *c)* $Ra = 10^6$ and $\varphi = 0$, *d)* $Ra = 10^6$ and $\varphi = \pi$

number, $Ta = \xi_0^2 H^4/\nu^2$ is the Taylor number.

The initial and boundary conditions are

$$\frac{\partial \omega_z}{\partial \tau} + u\frac{\partial \omega_z}{\partial x} + v\frac{\partial \omega_z}{\partial y} + w\frac{\partial \omega_z}{\partial z} - \omega_x\frac{\partial w}{\partial x} - \omega_y\frac{\partial w}{\partial y} - \omega_z\frac{\partial w}{\partial z} = \\ = \frac{1}{\sqrt{Ta}}\left(\frac{\partial^2 \omega_z}{\partial x^2} + \frac{\partial^2 \omega_z}{\partial y^2} + \frac{\partial^2 \omega_z}{\partial z^2}\right) + \frac{Ra}{Pr{\cdot}Ta}\left\{\frac{\partial \theta}{\partial x}\cos(\tau) - \frac{\partial \theta}{\partial y}\sin(\tau)\right\} - \frac{Ra_\xi}{Pr{\cdot}Ta}\left\{y\frac{\partial \theta}{\partial x} - x\frac{\partial \theta}{\partial y}\right\} + 2\frac{\partial w}{\partial z} \tag{9}$$

$$\frac{\partial \theta}{\partial \tau} + u\frac{\partial \theta}{\partial x} + v\frac{\partial \theta}{\partial y} + w\frac{\partial \theta}{\partial z} = \frac{1}{Pr{\cdot}\sqrt{Ta}}\left(\frac{\partial^2 \theta}{\partial x^2} + \frac{\partial^2 \theta}{\partial y^2} + \frac{\partial^2 \theta}{\partial z^2}\right) \tag{10}$$

Here $\mathrm{Ra} = g\beta\Delta T H^3/(a\nu)$ is the thermal Rayleigh number, $\mathrm{Ra}_\xi = \beta\Delta T H^4 \xi_0^2/(a\nu)$ is the rotational Rayleigh number, $Pr = \nu/a$ is the Prandtl

$$\tau = 0: \quad \psi_x = \psi_y = \psi_z = \omega_x = \omega_y = \omega_z = \theta = 0 \ \text{ for } -0.5 \le x \le 0.5, -0.5 \le y \le 0.5 \text{ and } -0.5 \le z \le 0.5;$$

$\tau > 0$:

$$\begin{aligned}
&\frac{\partial \psi_x}{\partial x} = \psi_y = \psi_z = 0, \quad \left| \begin{array}{l} \omega_x = 0, \\ \omega_y = -\partial w/\partial x, \\ \omega_z = \partial v/\partial x, \end{array} \right. \quad \theta = 0.5 \ \text{ for } \ x = -0.5, -0.5 \le y \le 0.5 \text{ and } -0.5 \le z \le 0.5; \\
&\frac{\partial \psi_x}{\partial x} = \psi_y = \psi_z = 0, \quad \left| \begin{array}{l} \omega_x = 0, \\ \omega_y = -\partial w/\partial x, \\ \omega_z = \partial v/\partial x, \end{array} \right. \quad \theta = -0.5 \ \text{ for } \ x = 0.5, -0.5 \le y \le 0.5 \text{ and } -0.5 \le z \le 0.5; \\
&\psi_x = \frac{\partial \psi_y}{\partial y} = \psi_z = 0, \quad \left| \begin{array}{l} \omega_x = \partial w/\partial y, \\ \omega_y = 0, \\ \omega_z = -\partial u/\partial y, \end{array} \right. \quad \frac{\partial \theta}{\partial y} = 0 \ \text{ for } \ y = \pm 0.5, -0.5 \le x \le 0.5 \text{ and } -0.5 \le z \le 0.5; \\
&\psi_x = \psi_y = \frac{\partial \psi_z}{\partial z} = 0, \quad \left| \begin{array}{l} \omega_x = -\partial v/\partial z, \\ \omega_y = \partial u/\partial z, \\ \omega_z = 0, \end{array} \right. \quad \frac{\partial \theta}{\partial z} = 0 \ \text{ for } \ z = \pm 0.5, -0.5 \le x \le 0.5 \text{ and } -0.5 \le y \le 0.5.
\end{aligned} \tag{11}$$

The average Nusselt number has been selected to describe the heat transference strength and defined as

$$\overline{Nu} = \int_{-0.5}^{0.5} \int_{-0.5}^{0.5} \left. \frac{\partial \theta}{\partial x} \right|_{x=-0.5} dydz \tag{12}$$

3. Numerical technique and validation

The control equations (6)–(10) with additional restrictions (11) have been solved by employing the finite difference procedures on the uniform mesh. The partial differential relations for the vector potential functions (6) have been discretized employing the seven-point difference schemes with central differences. The resulting equations have been worked out by the successive over-relaxation algorithm. Equations (7)–(10) have been solved using the locally one-dimensional Samarskii scheme where three-dimensional differential equation has been transformed to the set of one-dimensional equations along each coordinate. The central differences have been employed for diffusive terms and the Samarskii monotonic approximation is for the convective terms. The resulting difference equations have been solved by the tridiagonal matrix procedure. The mentioned algorithm has been programmed employing C++ programming language. To calculate the main characteristics of the fluid flow and heat transfer, the following algorithm has been used. First of all, all governing parameters including vector potential functions, vorticity, and temperature are initialized, then the parameters are calculated for a given time interval. For each time step, the following procedure is carried out, namely, definition of the velocity components using the relation between the velocity and vector potential functions, definition of vector potential functions using the Poisson equation (6), definition of vorticity components using differential equations (7)–(9), and definition of temperature employing the energy equation (10).

The presented computational model and in-house computational code have been validated successfully against the problem of convective heat transfers in a rotating cavity [29]. The comparison of the mean Nusselt number at the heated border for different time moments and various values of the mesh parameters is demonstrated in Table 1. The data obtained by other authors are well comparable with calculations. Moreover, Fig. 2 demonstrates comparison of temperature fields with data [29] at $Ra = 10^6$, $Ta = 10^6$, $Ra_\xi = 10^2$ for different cross-sections.

4. Results and discussion

The numerical data have been calculated for a wide range of control characteristics such as Prandtl number ($Pr = 0.7$), thermal Rayleigh number ($Ra = 10^3$–10^6), rotational Rayleigh number ($Ra_\xi = 0$–$1.8{\cdot}10^4$) and Taylor number ($Ta = 10^3$–10^6). Air has been chosen as a working fluid with $Pr = 0.7$. The range of the Rayleigh number corresponds to the temperature difference range for laminar regime with valid Boussinesq approximation. The considered range of Taylor number corresponds to the laminar and stable flow modes. The considered range of the rotational Rayleigh number has been defined using the values of the thermal Rayleigh number and Taylor number because $\mathrm{Ra}_\xi = \beta \Delta T H^4 \xi_0^2/(\alpha\nu)$. At the minimum values of the Rayleigh and Taylor numbers, convection is practically absent, which can be seen in the results. It should be noted that the rotational Rayleigh number is not independent and depends entirely on the choice of the Rayleigh number and the Taylor number. It is necessary to clarify that the outcomes have been received after numerous revolutions of the chamber to determine periodic nature of the flow structures and energy transport. The temperature distributions have been received during full cavity rotation. The influence of thermal Rayleigh number, rotational Rayleigh number and Taylor number has been illustrated employing the time evolution of the heat transfer strength.

Figs. 3 and 4 show three-dimensional temperature distributions for $Ra = 10^5$, $Ta = 10^4$, $Ra_\xi = 1.8{\cdot}10^2$ and various angles of rotation. Fig. 3 demonstrates temperature fields for cross-sections along z-coordinate, while Fig. 4 illustrates temperature fields along x-coordinate. In Fig. 3, at $\varphi = 0$, one can find a thermal plume extended along the upper adiabatic wall above the heated wall. A temperature spot of about 0.15 can be observed in Fig. 4 near the bottom part of the heated wall. Such a heat plume and heat spot characterize high heat removal from the heated surface, which can be seen in Fig. 5 showing the heat transfer rate. The thermal plume augments, since the medium rises up due to the buoyancy force impacts when the cavity is rotated to $\varphi = \pi/4$. It is realized due to the cavity rotates counter clockwise. At the same time, the cold zone of the medium tends to the heated border from the bottom zone of the chamber, which leads to an increase in the green temperature spot. Such a change in the temperature distribution characterizes the enhancement of heat removal. Further, the thermal plume and the spot begin to diminish when the cavity is rotated to the angle $\varphi = \pi/2$. This signals a downward trend in the average Nusselt number. At angles of rotation $\varphi = 3\pi/4$ and $\varphi = \pi$, the thermal plume is not so significant, while medium of a high temperature is located near the heated wall. The

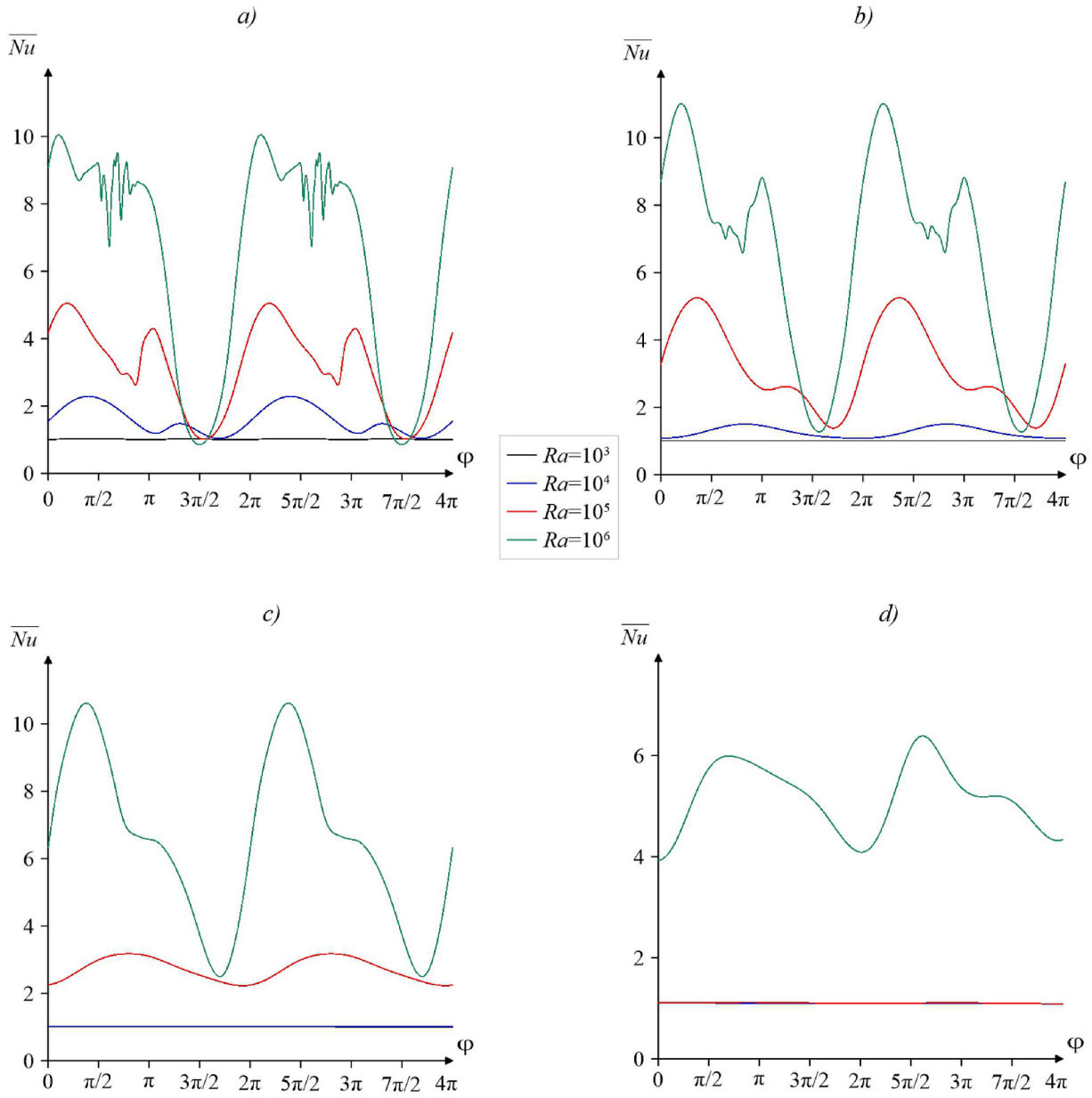

Fig. 6. Changes of $\overline{Nu}$ with *Ra* for various *Ta*: *a)* $Ta = 10^3$, *b)* $Ta = 10^4$, *c)* $Ta = 10^5$, *d)* $Ta = 10^6$ during two full revolutions of the cavity.

main part of the medium circulates in the center of the cavity and it does not mix the hot and cold parts. This temperature distribution characterizes a decrease in convective heat transfer, and heat removal occurs mainly due to the mechanisms of heat conduction. At the same time, low values of the mean *Nu* are observed. Then, the appearance of a thermal plume and a small short-term growth of the energy transport intensity at $5\varphi = \pi/4$ are observed again. At the angles of rotation $\varphi = 3\pi/2$ and $\varphi = 7\pi/4$, the temperature distributions again correspond to a regime with relatively low convection. The considered time interval is repeated after a complete revolution of the cavity.

Fig. 5 illustrates velocity patterns for different values of *Ra* and rotating angle for $Ta = 10^3$. The rotation of the cavity from $\varphi = 0$ to $\varphi = \pi$ leads to a change in the direction of the fluid flow and a decrease in the intensity. This is due to the opposite direction of rotation and buoyancy forces (due to the heating from the definite wall). A decrease in the flow rate characterizes a suppression of the energy transport processes. This can be observed in changes in the value of the Nusselt number. Then the flow can be changed by direction. Both the directions of rotation and the buoyancy force coincide towards the end of the rotation, which leads to the heat transfer enhancement. A rise of the Rayleigh number leads to a significant increase in the fluid flow rate, but such flow intensification does not change the flow structure significantly.

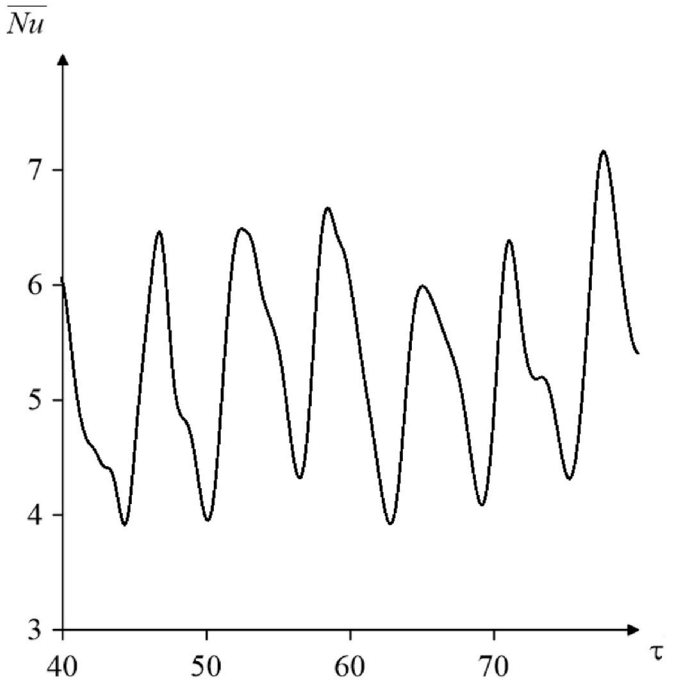

Fig. 7. Changes of $\overline{Nu}$ for $Ta = 10^6$ and $Ra = 10^6$.

Fig. 6 illustrates effect of *Ra* for various values of *Ta* on average Nusselt number at heated wall. As mentioned earlier, the results have been obtained for a cavity that made a sufficient number of revolutions to achieve periodicity in the flow structures and temperature fields. This can be seen in the repeated magnitudes of average *Nu* in two subsequent revolutions of the cavity, except for the case *d)* $Ra = 10^6$. The behavior of the liquid circulation and energy transport is non-periodic when the cavity has a high rotation speed and a large temperature difference between the walls. A growth of the Rayleigh number results in an augmentation of energy transport due to buoyancy force (see Fig. 6*a*). The minimum magnitudes of *Nu* remain at the same value, while the maximum values increase with *Ra*. The same nature can be said about case *b)*, except for that the amplitude of changes in the Nusselt number decreases. More clearly in case *c)*, identical results for the average Nusselt number can be found for $Ra = 10^3$ and $Ra = 10^4$. In case *d)*, a raise of *Ra* from 10^3 till 10^5 does not lead to an enhancement of energy transfer due to a strong influence of the rotation. It can be concluded that an increment of the angular rate of the rotating chamber characterizes a suppression of the convective heat transfer within this cavity and as a result an influence of the Rayleigh number is not significant.

Fig. 7 demonstrates the change of average Nusselt number during several rotations of the cavity for $Ta = 10^6$ and $Ra = 10^6$. Values of average *Nu* does not repeat at any cavity turn due to non-periodic changes in thermo-hydrodynamic. On the other hand, amount of minimum and maximum values coincide with amount of cavity turns. This behavior can be called « chaotic oscillation». Such results can be obtained for high values of Rayleigh and Taylor numbers. For example, similar effect has been obtained by Jin et al. [7] for rotating rectangular cavity.

Fig. 8 illustrates the effect of Taylor number for various *Ra*. An increment of the angular velocity results in a decrease in convective heat transfer rate for all results, except for the case of $Ta = 10^6$ at low *Ra* (10^3 and 10^4). In the case of low Rayleigh number value (see Fig. 8*a*), a change of the Taylor number does not lead to significant changes in $\overline{Nu}$. The difference between two extremums of average *Nu* is insignificant and less than 4% when $Ta = 10^3$. An intensification of heat transfer can be observed at moderate rotation rates $Ta = 10^3$ and $Ta = 10^4$ in case *b)*. A further increase in the amplitude can be observed in cases *c)* and *d)*. It can be concluded that marked influence of the Taylor number occurs for high *Ra*. An interesting result can be found for $Ta = 10^6$ when $Ra = 10^3$ and $Ra = 10^4$, namely, a growth of $\overline{Nu}$ with *Ta* between 10^5 and 10^6. Such behavior can be explained by a strengthening of the heat conduction.

Time-averaged Nusselt number values during full revolution of the cavity for different values of the Rayleigh and Taylor numbers are demonstrated in Table 2. As shown earlier, regardless of the Taylor number values an increase in the Rayleigh number leads to an intensification of heat transfer. At the same time, an increase in the rotation speed of the cavity leads to the suppression of convection, except for high *Ra*, where it is possible to strengthen the heat transfer for $Ra = 10^6$ with the Taylor number. Such behavior can be explained by a formation of the transitional period for *Ra* and *Ta*.

The influence of the centrifugal force is demonstrated in Fig. 9 by changing the average Nusselt number during two full revolutions of the cavity for various magnitudes of the control characteristics. The rotational *Ra* is dependent on other determined parameters. While the physical properties of the medium and the characteristic dimensions of the cavity are fixed, the magnitude of the rotational *Ra* depends on the rotation speed of the cavity ξ_0 (or the Taylor number, respectively).

Fig. 9 shows comparison of the results with and without centrifugal force. In the case *a*) for $Ta = 10^4$, a change of the thermal Rayleigh number does not lead to variations of the results, which means that the influence of the rotational Rayleigh number is insignificant for the considered range of the thermal Rayleigh number and $Ta = 10^4$. In the case *b*) for $Ra = 10^5$, a change of the Taylor number results in an appearance of difference in the results only for the case of intense rotation when $Ta = 10^6$. The result obtained for $Ta = 10^6$ and different values of Ra_ξ can be explained by studied the motion equations. The values of the diffusion terms and the buoyancy force decrease with an increase in the Taylor number, since Taylor number is in the denominator. On the other hand, the rotational Rayleigh number increases with a growth of the angular velocity (or with a raise of the Taylor number) and located in the numerator of the rotational buoyancy force. As a result, the centrifugal force term makes a larger contribution to the equation. But as the results showed, this effect is insignificant.

Fig. 10 demonstrates the change of the average Nusselt number during two full cavity revolutions for two-dimensional and three-dimensional modeling at different values of governing parameters. Good agreement of the results has been obtained at low convective heat transfer modes. This is the case of $Ra = 10^3$, when there is a low temperature difference between the heated and cooled walls, and the case of $Ta = 10^6$, when the high rotational velocity suppressed the convective heat transfer. A quantitative difference in the average Nusselt number has been observed for modes with a small oscillation amplitude at $Ra = 10^4$ and $Ta = 10^5$. In the case of more intense fluid flows $Ra = 10^5$, $Ra = 10^6$ and $Ta = 10^3$, $Ta = 10^4$, the results may coincide or differ depending

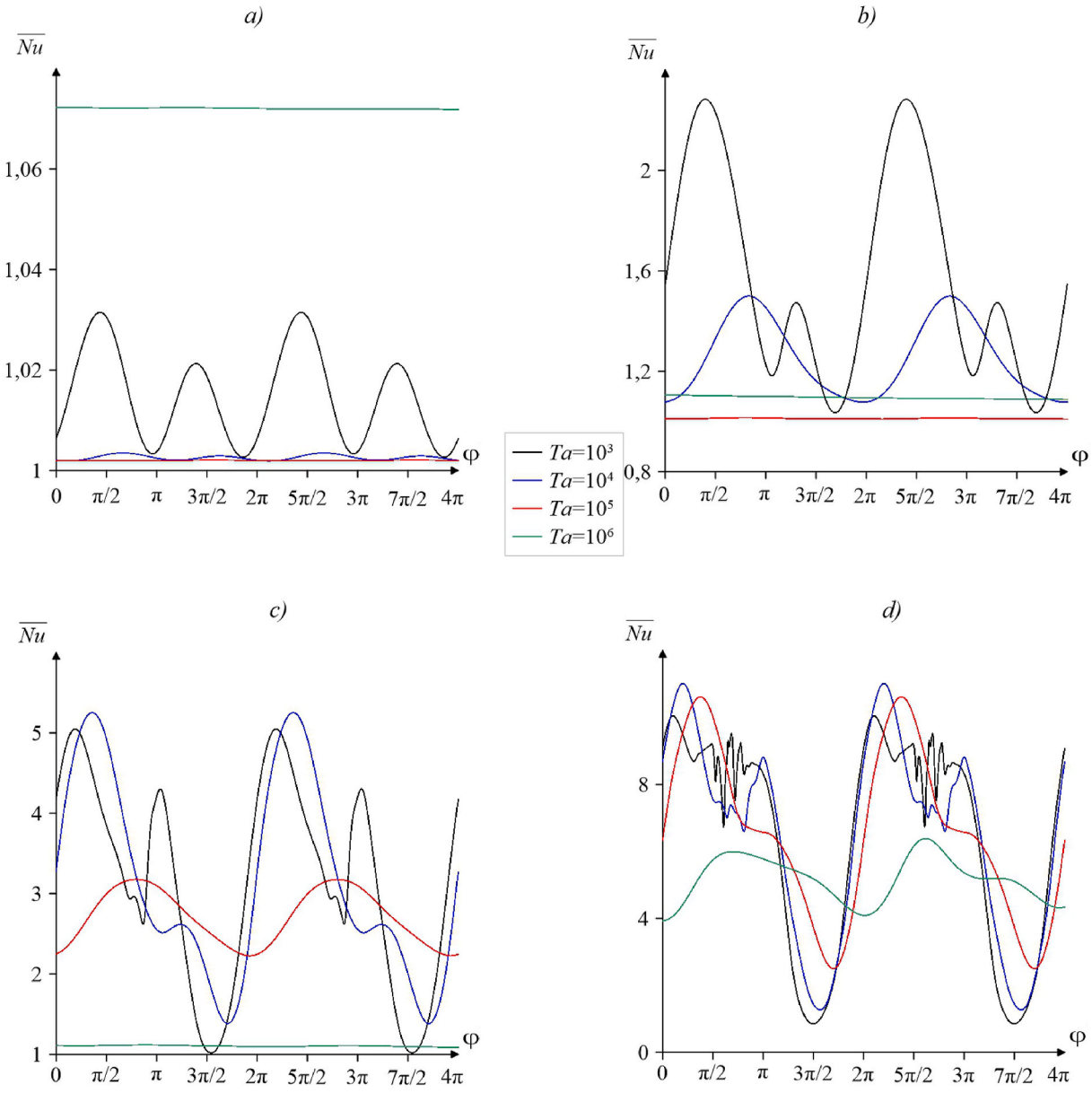

Fig. 8. Variations of average *Nu* on Taylor number for different *Ra*: *a)* $Ra = 10^3$, *b)* $Ra = 10^4$, *c)* $Ra = 10^5$, *d)* $Ra = 10^6$ during two full revolutions of the cavity.

Table 2
Time-averaged Nusselt number values with different *Ra* and *Ta*.

	$Ta = 10^3$	$Ta = 10^4$	$Ta = 10^5$
$Ra = 10^3$	1.01465	1.0024	1.00233
$Ra = 10^4$	1.5807	1.25567	1.01121
$Ra = 10^5$	3.15273	3.15769	2.71374
$Ra = 10^6$	6.41137	6.4683	6.53866

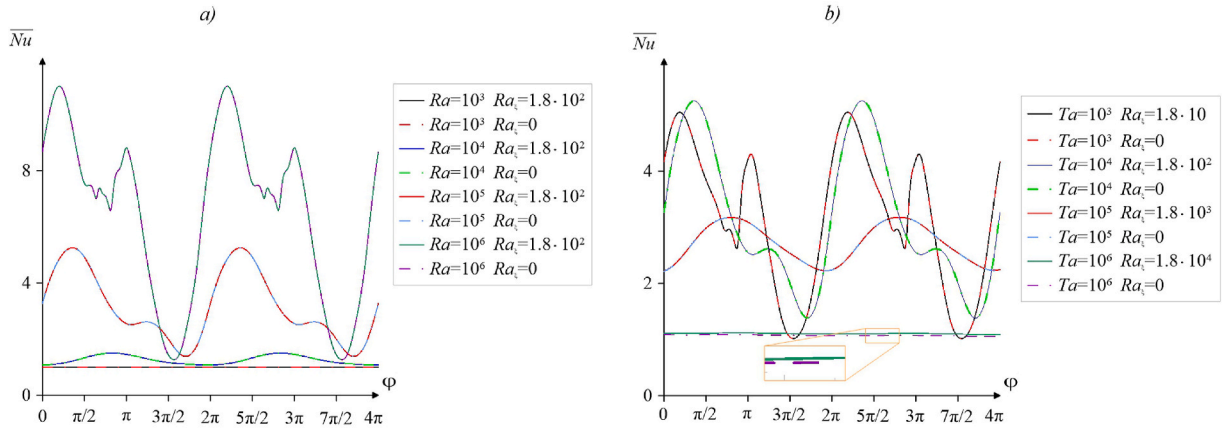

Fig. 9. Changes of average *Nu* with rotational *Ra* for *a*) $Ta = 10^4$ and different Rayleigh numbers, *b*) $Ra = 10^5$ and different Taylor numbers during two full revolutions of the chamber.

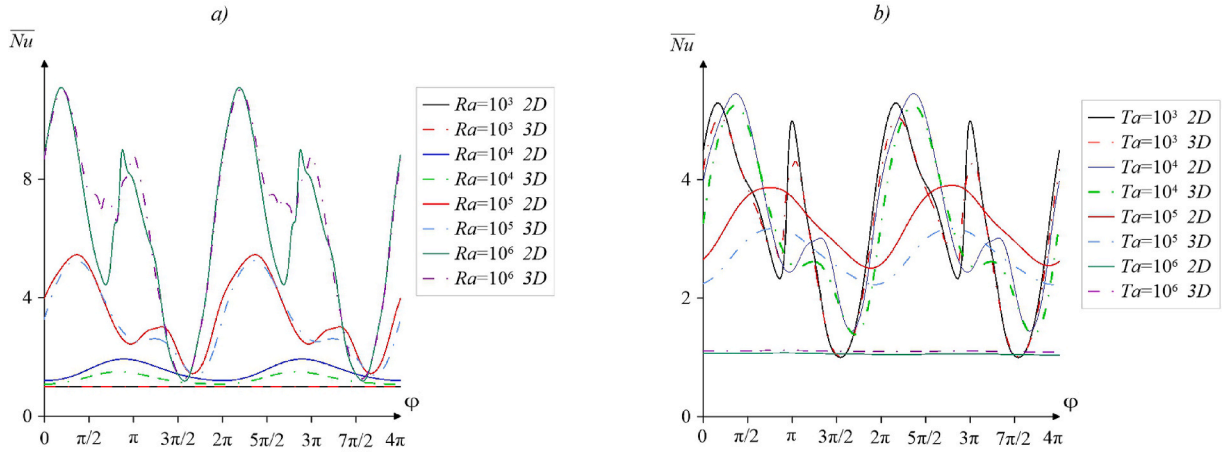

Fig. 10. Changes of mean *Nu* with the considered model dimension for *a*) $Ta = 10^4$ and different Rayleigh numbers, *b*) $Ra = 10^5$ and different Taylor numbers during two full revolutions of the cavity.

on the angle of rotation during cavity revolution. For example, a difference has been observed due to the restructuring of the fluid flow for $Ra = 10^6$ with rotation from $\pi/2$ to π, while a good comparison of the results has been observed at other angles of the cavity rotation.

Fig. 11 shows a comparison of temperature fields for three-dimensional and two-dimensional computational models. The temperature fields for the three-dimensional model are presented for the plane $z = 0$. The isotherms coincide well near the heated and cooled walls for all angles of cavity rotation. The isotherms in the center of the cavity may not coincide and cross, for example, at $\varphi = 5\pi/4$ and $\varphi = 7\pi/4$. The difference can also be observed when more complex structures of temperature distributions arise. For example, the displacement of the convective cells cores has been observed at $\varphi = 3\pi/4$. Comparison of 2D and 3D simulation results is an interesting issue and will be explored in more detail for various aspect ratios in future studies as presented earlier [30–33].

5. Conclusions

Convective energy transference in a differentially warmed rolling cubical cavity has been studied. A computational dimensionless model has been solved by using the finite difference method of the second-order accuracy with the uniform mesh. The temperature fields for full cavity rotation have been analyzed. The influences of thermal Rayleigh number, rotational Rayleigh number and Taylor number have been illustrated using the mean *Nu*. The effect of the centrifugal force has been described. The outcomes have been compared with the data of two-dimensional modeling. Based on the findings, the main conclusions are as follows:

- A raise of the angular velocity of the cavity results in a reduction of the thermal Rayleigh number influence. It means that an increment of *Ta* suppresses the convective heat transfer.

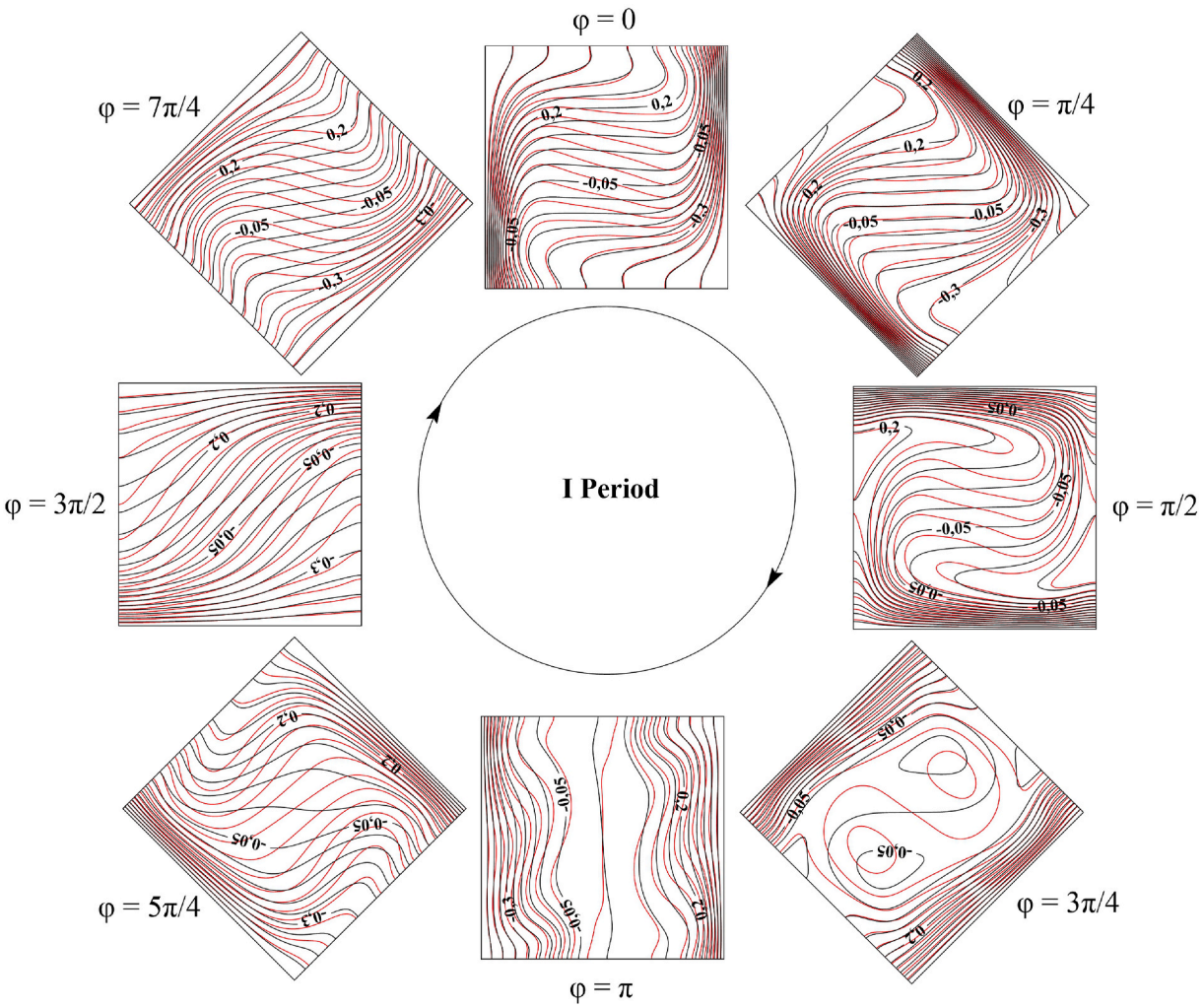

Fig. 11. Temperature fields for three-dimensional (black lines) and two-dimensional (red lines) models at $Ta = 10^4$ and $Ra = 10^5$ and different angles of the cavity rotation.

- An increase in the temperature drop between the isothermal walls results in an increment of the effect of rotation on energy transport.
- The most intense heat transfer can be achieved at high Rayleigh and Taylor numbers.
- The effect of the centrifugal force is insignificant for the case of Boussinesq approximation when the Boussinesq number is low.
- In the case of cubical cavity, the results of the two-dimensional approach for the square cavity can be the first approximation, but it is necessary to study an influence of the aspect ratio on this comparison.

Declaration of competing interest

The authors declare that they have no known competing financial interests or personal relationships that could have appeared to influence the work reported in this paper.

Data availability

Data will be made available on request.

Acknowledgement

The reported study was funded by the Russian Foundation for Basic Research according to the research project N⁰ 20-31-90081.

References

[1] S.-C. Huang, C.-C. Wang, Y.-H. Liu, Heat transfer measurement in a rotating cooling channel with staggered and inline pin-fin arrays using liquid crystal and stroboscopy, Int. J. Heat Mass Tran. 115 (2017) 364–376, https://doi.org/10.1016/j.ijheatmasstransfer.2017.07.040.

[2] C. Le, L. Liu, Z. Li, Numerical investigation of the effect of rotation on the oscillatory thermocapillary convection and dopant transport in a silicon liquid bridge, J. Cryst. Growth 523 (2019) 125149, https://doi.org/10.1016/j.jcrysgro.2019.125149.

[3] W. Wu, L. Amsbeck, R. Buck, N. Waibel, P. Langner, R. Pitz-Paal, On the influence of rotation on thermal convection in a rotating cavity for solar receiver applications, Appl. Therm. Eng. 70 (1) (2014) 694–704, https://doi.org/10.1016/j.applthermaleng.2014.03.059.

[4] R. Chokri, B.-B. Brahim, Three-dimensional natural convection of molten Lithium in a differentially heated rotating cubic cavity about a vertical ridge, Powder Technol. 291 (2016) 97–109, https://doi.org/10.1016/j.powtec.2015.12.010.

[5] L.F. Jin, K.W. Tou, C.P. Tso, Experimental and numerical studies on a rotating cavity with discrete heat sources with conjugate effects, Exp. Heat Tran. 18 (2005) 259–277, https://doi.org/10.1080/08916150500201552.

[6] C.P. Tso, L.F. Jin, K.W. Tou, Numerical segregation of the effects of body forces in a rotating, differentially heated enclosure, Numer. Heat Tran., Part A: Applications 51 (2007) 85–107, https://doi.org/10.1080/10407780600710318.

[7] L.F. Jin, K.W. Tou, C.P. Tso, Effects of rotation on natural convection cooling from three rows of heat sources in a rectangular cavity, Int. J. Heat Mass Tran. 28 (19–20) (2007) 3982–3994, https://doi.org/10.1016/j.ijheatmasstransfer.2005.04.013.

[8] N. Al-Zurfi, A. Alhusseny, A. Nasser, Effect of rotation on forced convection in wavy wall channels, Int. J. Heat Mass Tran. 149 (2020) 119177, https://doi.org/10.1016/j.ijheatmasstransfer.2019.119177.

[9] Z. Tao, L. Qiu, H. Deng, Heat transfer in a rotating smooth wedge-shaped channel with lateral fluid extraction, Appl. Therm. Eng. 87 (2015) 47–55, https://doi.org/10.1016/j.applthermaleng.2015.04.073.
[10] R.K. Vanishree, P.G. Siddheshwar, Effect of rotation on thermal convection in an anisotropic porous medium with temperature-dependent viscosity, Transport Porous Media 81 (1) (2010) 73–87, https://doi.org/10.1007/s11242-009-9385-2.
[11] P. Vadasz, Coriolis effect on free convection in a long rotating porous box subject to uniform heat generation, Int. J. Heat Mass Tran. 38 (11) (1995) 2011–2018, https://doi.org/10.1016/0017-9310(94)00313-K.
[12] S. Govender, P. Vadasz, The effect of mechanical and thermal anisotropy on the stability of gravity driven convection in rotating porous media in the presence of thermal non-equilibrium, Transport Porous Media 69 (2007) 55–66, https://doi.org/10.1007/s11242-006-9063-6.
[13] D. Yadav, The effect of viscosity and Darcy number on the start of convective motion in a rotating porous medium layer saturated by a couple-stress fluid, Proc. IME C J. Mech. Eng. Sci. 235 (6) (2021) 999–1007, https://doi.org/10.1177/0954406220942551.
[14] D. Yadav, Numerical examination of the thermal instability in an anisotropic porous medium layer subjected to rotation and variable gravity field, Special Top. Rev. Porous Media 11 (4) (2020) 395–407, https://doi.org/10.1615/SPECIALTOPICSREVPOROUSMEDIA.2020031484.
[15] D. Yadav, Effects of rotation and varying gravity on the onset of convection in a porous medium layer: a numerical study, World J. Eng. 17 (6) (2020) 785–793, https://doi.org/10.1108/WJE-03-2020-0086.
[16] A. Hussain, M.A. Elkotb, M. Arshad, A. Rehman, K. Sooppy Nisar, A. Hassan, C. A. Saleel, Computational investigation of the combined impact of nonlinear radiation and magnetic field on three-dimensional rotational nanofluid flow across a stretchy surface, Processes 9 (2021) 1453, https://doi.org/10.3390/pr9081453.
[17] A. Sohankar, A. Joulaei, M. Mahmoodi, Fluid flow and convective heat transfer in a rotating rectangular microchannel with various aspect ratios, Int. J. Therm. Sci. 172 (2022) 107259, https://doi.org/10.1016/j.ijthermalsci.2021.107259.
[18] S. Shekhar, R. Ragoju, G.J. Reddy, M.A. Sheremet, The Coriolis effect on thermal convection in a rotating sparsely packed porous layer in presence of cross-diffusion, Coatings 12 (2022) 23, https://doi.org/10.3390/coatings12010023.
[19] A.S. Alshomrani, S. Sivasankaran, A.A. Ahmed, Numerical study on convective flow and heat transfer in 3D inclined enclosure with hot solid body and discrete cooling, Int. J. Numer. Methods Heat Fluid Flow 30 (10) (2020) 4649–4659, https://doi.org/10.1108/hff-09-2019-0692.
[20] A.S. Alshomrani, S. Sivasankaran, A.A. Amer, A. Biswas, Numerical study on convective flow in a three-dimensional enclosure with hot solid body and discrete cooling, Numer. Heat Tran., Part A: Applications 76 (2) (2019) 87–99, https://doi.org/10.1080/10407782.2019.1618626.
[21] L. Kolsi, F. Selimefendigil, H.F. Öztop, W. Hassen, W. Aich, Impacts of double rotating cylinders on the forced convection of hybrid nanofluid in a bifurcating channel with partly porous layers, Case Stud. Therm. Eng. 26 (2021) 101020, https://doi.org/10.1016/j.csite.2021.101020.
[22] N. Shirani, D. Toghraie, Numerical investigation of transient mixed convection of nanofluid in a cavity with non-Darcy porous inner block and rotating cylinders with harmonic motion, Sci. Rep. 11 (2021) 17281, https://doi.org/10.1038/s41598-021-96733-6.
[23] K. Yang, K. Liu, J. Wang, Pore-scale numerical simulation of convection heat transfer in high porosity open-cell metal foam under rotating conditions, Appl. Therm. Eng. 195 (2021) 117168, https://doi.org/10.1016/j.applthermaleng.2021.117168.
[24] Y.T. Ker, T.F. Lin, A combined numerical and experimental study of air convection in a differentially heated rotating cubic cavity, Int. J. Heat Mass Tran. 39 (15) (1996) 3193–3210, https://doi.org/10.1016/0017-9310(95)00404-1.
[25] S.W. Chang, T. Liou, T.L. Yang, G.F. Hong, Heat transfer in radially rotating pin-fin channel at high rotation numbers, J. Turbomach. 132 (2) (2010), 021019, https://doi.org/10.1115/1.3147103.
[26] Y.-H. Liu, M. Huh, J.-C. Han, High rotation number effect on heat transfer in a trailing edge channel with tapered ribs, Int. J. Heat Fluid Flow 33 (1) (2012) 182–192, https://doi.org/10.1016/j.ijheatfluidflow.2011.10.002.
[27] H. Deng, Y. Cheng, Y. Li, B. Ni, L. Qiu, Heat transfer in a two-inlet rotating wedge-shaped channel with various locations of the second inlet, Int. J. Heat Mass Tran. 106 (2017) 25–34, https://doi.org/10.1016/j.ijheatmasstransfer.2016.10.049.
[28] X. Yang, Z. Ren, X. Li, J. Ren, P.M. Ligrani, Flow and heat transfer characteristics in a pre-swirl rotor-stator cavity, Int. J. Therm. Sci. 172 (2022) 107271, https://doi.org/10.1016/j.ijthermalsci.2021.107271.
[29] T.L. Lee, T.F. Lin, Transient three-dimensional convection of air in a differentially heated rotating cubic cavity, Int. J. Heat Mass Tran. 39 (6) (1996) 1243–1255, https://doi.org/10.1016/0017-9310(95)00193-X.
[30] V.I. Terekhov, A.L. Ekaid, Three-dimensional laminar convection in a parallelepiped with heating of two side walls, High Temp. 49 (6) (2011) 874–880, https://doi.org/10.1134/S0018151X11060228.
[31] S.G. Martyushev, I.V. Miroshnichenko, M.A. Sheremet, Influence of the geometric parameter on the regimes of natural convection and thermal surface radiation in a closed parallelepiped, J. Eng. Phys. Thermophys. 88 (6) (2015) 1522–1529, https://doi.org/10.1007/s10891-015-1338-8.
[32] N.S. Bondareva, M.A. Sheremet, Influence of uniform magnetic field on laminar regimes of natural convection in an enclosure, Thermophys. Aeromechanics 22 (2) (2015) 203–216, https://doi.org/10.1134/S0869864315020079.
[33] M.S. Astanina, B. Buonomo, O. Manca, M.A. Sheremet, Effect of third size on natural convection of variable viscosity fluid in a closed parallelepiped, Int. Commun. Heat Mass Tran. 128 (2021) 105618, https://doi.org/10.1016/j.icheatmasstransfer.2021.105618.